Eng. Sci., 2021, **14**, 46–58

Engineered Science

DOI: https://dx.doi.org/10.30919/es8d1160

Thionaphthoquinones as Photosensitizers for TiO_2 Nanorods and ZnO Nanograin Based Dye-sensitized Solar Cells: Effect of Nanostructures on Charge Transport and Photovoltaic Performance

Sharad A. Mahadik,[1, 2] Amit Patil,[1] Habib M. Pathan,[2,*] Sunita Salunke-Gawali[1,*] and Ray J. Butcher[3]

Abstract

Two analogs of thionaphthoquinone dyes, viz; AMT; 2-((thiophen-2-yl)methylamino)-3-chloro-naphthalene-1,4-dione and AET;2-((thiophen-2-yl)ethylamino)-3-chloro-naphthalene-1,4-dione are synthesized from 2,3-dichloronaphthalene-1,4-dione and were used as light harvester in the TiO_2 and ZnO based dye-sensitized solar cells (DSSC's). FT-IR analysis of AMT and AET showed N-H band's existence at 3316 cm^{-1} and 3269 cm^{-1}, respectively. X-Ray Crystallographic Data Collection and Refinement confirms the AMT crystallizes in monoclinic space group *P2/c*. The optical properties of the photosensitizers loaded ZnO shows the broadband in the UV region assigned to $\pi \rightarrow \pi^*$ transition while a visible region band assigned to $n \rightarrow \pi^*$ charge transfer transition. The photovoltaic performances of thionaphthoquinone photosensitizers in TiO_2 nanorod and ZnO nanograin based electrodes were studied and compared. Electrochemical impedance analysis reveals the higher electron transport rate in ZnO, but the improved efficiency of TiO_2 based DSSC is due to the higher dye loading and fast electron injection. The power conversion efficiencies of the DSSC's fabricated using AMT and AET photosensitizers on ZnO and TiO_2NR (NR = nanorod) electrodes are 0.02, 0.03, and 0.23, 0.32 %, respectively. The hydrothermally deposited TiO_2nanorod arrays exhibited the highest performance over doctor blade method deposited ZnO based DSSC's. The present study will open a new route to fabricate highly efficient DSSC's using morphologically dependent photoelectrode.

Keywords: Thionaphthoquinones: Electron-hole pair recombination; Dye-sensitized solar cells; Zinc oxide (ZnO); TiO_2 nanorod.
Received: 12 November 2020; Accepted: 14 December 2020.
Article type: Research article.

1. Introduction

Since the first report on TiO_2-based dye-sensitized solar cells (DSSCs) by O'Regan and Grätzel,[1] due to relatively high potentials like solar energy conversion efficiency, easy manufacture, and their low cost, DSSCs have been considered as one of the excellent candidates for a new renewable energy source.[2] Nickel cobalt sulfide ($NiCo_2S_4$), Copper hydroxide ($Cu(OH)_2$) are eco-friendly, low-cost materials used in supercapacitors for energy storage applications.[3,4] DSSCs are a third-generation solar cell that works similar to photosynthesis in which different sensitizers are used for absorption of light energy.[5] Grätzel and co-workers reported that the high-efficiency DSSCs consist of a Ruthenium (II) based light absorbing sensitizer loaded nanocrystalline TiO_2 photoanode, redox couple I^-/I_3^- as an electrolyte, and platinized conducting glass as counter electrode.[6,7] None the less, Ruthenium (II) based dyes have provided a relatively high efficiency; however, there are several drawbacks of them such as the durability due to the presence of two or three NCS groups, high cost, the rarity of noble metals, and lower molar extinction coefficients above 600 nm.[8] Several researchers attempted the synthesis and loading of metal-free organic dyes in DSSC's to replace Ru (II) based dyes[9] to address these issues. Metal-free organic dyes such as 9-phenylxanthene dyes (*e.g.*, Rhodamine B dye, rose Bengal dye and fluorescein

[1] *Department of Chemistry, Savitribai Phule Pune University, Pune, India-411007.*
[2] *Advanced Physics Laboratory, Department of Physics, Savitribai Phule Pune University, Pune, India-411007.*
[3] *Department of Chemistry, Howard University, Washington, D.C, 20059, USA.*
* *E-mail:* pathan@physics.unipune.ac.in (H. M. Pathan), sunitasalunke@rediffmail.com (S. Salunke-Gawali)

dye, *etc.*) are also used as photosensitizers for DSSC's and studied their solar cell properties.[10–13] However, besides the sensitizers, several other parameters affect the photovoltaic performance of the DSSC's such as photochemically stable semiconductor materials, molar absorption coefficient, electrolyte performance for the regeneration of photosensitizer and sheet resistance of the conducting transparent substrates, *etc*.[14-17] Additionally, as the high viscosity of redox electrolyte containing iodide and triiodide (I^-/I_3^-) ions,[18] the diffusion of I^- and I_3^- ions in ionic liquids is slow, and therefore to reach a high conversion efficiency of DSSC's, thin, porous electrodes, a high-extinction-coefficient dye should be needed.[19] Despite electrolyte, the current research is going on to enhancing the efficiency of DSSC by replacing standard Ru-based dyes with organic dyes and developing photoanodes with various morphologies and metal oxide semiconductors such as zinc oxide (ZnO), TiO_2 and tin oxide (SnO_2).[20-24]

The power conversion efficiency of 11–13% under the simulated one sun illumination has been reported via polypyridyl and porphyrin complexes of ruthenium or zinc and dyes with carboxy-anchor moieties for binding to the surface of the TiO_2.[25,26] Therefore, the fabrication of DSSCs with a power conversion efficiency of over 14% has attracted considerable interest from numerous research communities.[27] As the morphology and structure of the photoanode have a crucial role in reducing charge recombination, promoting electron transport, and increasing charge collection efficiency, selecting the electrode material is one of the critical parameters in DSSCs. Therefore, an attempt has been made to develop the DSSC's with novel photosensitizers and ZnO and TiO_2 based photoelectrodes with different structure and morphology. Besides, the photosensitizers are derivatives of naphthoquinone and act as a chemosensor property; these are redox-active compound, these compounds absorb light in UV region ($\pi \rightarrow \pi^*$) transition and visible region ($n \rightarrow \pi^*$) transition.[28,29] The AMT and AET act as donor-π-accepter (D-π-A) dye structures during the DSSC working. In our previous work, the 2R-(***n***-alkylamino)-1,4-naphthoquinone were used as a photosensitizer for the mesoporous ZnO based photoelectrodes. The 2R-(*n*-alkylamino)-1,4-naphthoquinone photosensitizer loaded mesoporous ZnO photoelectrodes showed better power conversion efficiency with less recombination between photoanode/electrolyte interface and higher electron lifetime than the other photosensitizers.[30] Therefore attempts have been made to form a novel AMT and AET sensitized ZnO nanograin and TiO_2 based DSSC's.

In this investigation, we have designed and synthesized novel two analogs of thionaphthoquinones dyes, viz; AMT; 2-((thiophen-2-yl)methylamino)-3-chloro-naphthalene-1,4-dione, AET; 2-((thiophen-2-yl)ethylamino)-3-chloro-naphthalene-1,4-dione. The molecular structures of photosensitizers (AMT and AET) are shown in Fig.1. We used a doctor blade method and hydrothermal technique to fabricate ZnO nanograin and TiO_2 nanorod arrays electrodes. Further electrodes were analyzed for their structural, morphological, and optical properties. Dye-sensitized solar cells are developed by loading thionaphthoquinones photosensitizer solutions as AMT and AET on the ZnO and TiO_2 based photoelectrodes in a separate set of experiments. Depending upon AET and AMT's choice, the ZnO and TiO_2 based electrodes are named ZnO/AMT, ZnO/AET, TiO_2NR/AMT, TiO_2NR/AET, respectively. Further, device characteristics in terms of the photocurrent, carrier recombination, and transport times of the fabricated photoanodes (ZnO/AMT, ZnO/AET, TiO_2NR/AMT, and TiO_2NR/AET) are investigated in detail. EIS results of the AET photosensitizer loaded on ZnO/AET photoelectrode exhibited lower charge transfer resistance (R2) than AMT, suggesting less recombination between photoanode/electrolyte interface and higher electron lifetime than the (ZnO/AMT, TiO_2NR/AET, and TiO_2NR/AMT). Comparing the optimum ZnO nanograin and TiO_2NR based DSSC's photoelectrochemical properties, the best device efficiency is achieved for the AET photosensitized TiO_2NR (TiO_2NR/AET) electrodes (0.32 %). The present study provides a mechanistic explanation for the dye conjugation and development of organic (AMT, AET) sensitized ZnO and TiO_2NR based DSSC's.

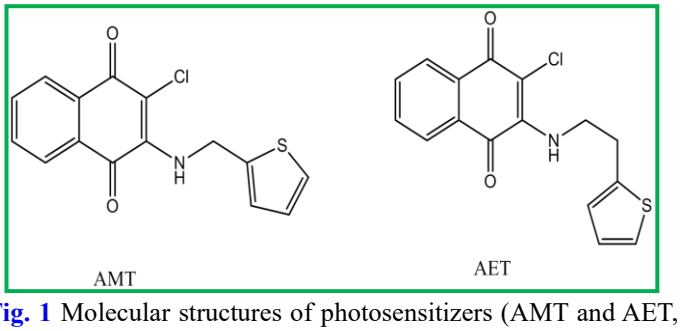

Fig. 1 Molecular structures of photosensitizers (AMT and AET, respectively).

2. Experimental

2.1 Materials and methods

The materials used viz 2,3-dichloronaphthalene-1,4-dione were purchased from Sigma-Aldrich. Dichloromethane (AR), Toluene (LR), Methanol (AR), Ethanol (AR) were purchased from Merck Chemicals. Toluene was distilled by standard methods,[31] and dry methanol was prepared by the literature reported procedure.[32] Thiophen-2-ylmethanamine (AR), Titanium butoxide, Hydrochloric acid, 2-(thiophen-2-yl)ethanamine (AR), ZnO powder (Sigma-Aldrich), ethylcellulose (SRL), α-terpineol obtained from HPCL, and acetylacetone (SRL) was used as received.

2. 2 General procedure for the synthesis of photosensitizers

2-((thiophen-2-yl)methylamino)-3-chloro-naphthalene-1,4-dione (AMT) and 2-((thiophen-2-yl)ethylamino)-3-chloro-naphthalene-1,4-dione (AET) was synthesized by using Scheme 1(a,b). Specifically, 1 g of 2,3-dichloronaphthalene-1,4-dione (4.40 mmol) was dissolved in 25 ml dichloromethane. Further, the solution was kept stirring for 30 min at room temperature (26°C). The required amount of

thiophen-2-ylmethanamine/2-(thiophen-2-yl)ethanamine (4.40 mmol) was added dropwise with constant magnetic stirring. The reaction mixture was further stirred for 12 h at room temperature (26 °C). Further, the color of the reaction mixture was turned from yellow to orange. The product obtained was evaporated in air and purified by exhaustive column chromatography (Solvent system 100 % toluene).

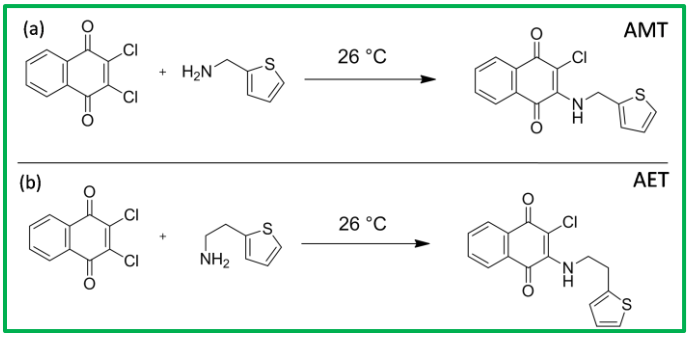

Scheme 1 Scheme 1 (a) Synthesis of photosensitizer AMT (from left to right) respectively 2,3-dichloronaphthalene-1,4-dione, thiophen-2-ylmethanamine, 2-((thiophen-2-yl)methylamino)-3-chloro-naphthalene-1,4-dione, (b) Synthesis of photosensitizer AET (from left to right) respectively 2,3-dichloronaphthalene-1,4-dione,2-(thiophen-2-yl)ethanamine, 2-((thiophen-2-yl)ethylamino)-3-chloro-naphthalene-1,4-dione (photosensitizer AET).

2.3 Characterization of AMT and AET

FT-IR spectra of AMT and AET recorded between 4000 and 400 cm^{-1} as ATR Spectrophotometer (Fig. S1 and Fig. S2 in ESI†). Melting points (mp) of compounds were determined using the melting point apparatus (Make- METTER) and by DSC; (Differential Scanning Calorimetry) recorded on SHIMADZU, Make-TA Q2000; Tzero aluminum pan used as sample holder in DSC studies (Fig. S3 and Fig. S4 in ESI†). ^{1}H (400 MHz) and ^{13}C (100 MHz) NMR of all compounds were recorded in DMSO-d6 on Varian NMR instrument. TMS (tetramethylsilane) was used as the reference in the $CDCl_3$ solvent, while the spectra recorded in DMSO-d_6 are calibrated with solvent peak δ = 2.5 ppm (Fig. S5, Fig. 6 and Fig. S7, Fig. S8 in ESI†). The mass of the AMT and AET was determined by the Liquid chromatograph-mass spectrum (LC-MS) recorded on Bruker mass spectrometer (Make: IMPACT II UHR-TOF, Ultra-High-Resolution Time-Of-Flight) (Fig. S9 and Fig. S10 in ESI†).

2.4 X-Ray Crystallographic Data Collection and Refinement of the Structures

X-ray quality crystal AMT was obtained after the evaporation of methanol solvent. The crystal of the appropriate size was chosen for data collection. Data for AMT were collected on D8 venture PHOTON 100 CMOS diffractometer using graphite Monochromated Mo-Kα radiation (λ = 0.71073Å) from a Mo-target rotating-anode X-ray source was used. Final cell constants obtained from the least-squares fit of several thousand strong reflections. Intensity data corrected for absorption using intensities of redundant reflection with the program SADAB.[33-34] The structure was solved readily by direct methods and subsequent difference Fourier techniques. The Siemens ShelXTL[35-37] software package used for a solution and Mercury 3.8 for the structures' artwork, SHELXL2018/3, based on F^2, was used to refine the structures. All non-hydrogen atoms anisotropically refined, and hydrogen atoms were placed at the calculated position and refined as riding atoms with isotropic displacement parameters. The crystallographic parameters for AMT can be represented in Table S1-S8 in ESI†. Crystallographic data have been deposited with the Cambridge Crystallographic Data Centre (CCDC). They may be obtained on request quoting the CCDC deposition number 2042885 from the CCDC, 12 Union Road, Cambridge CB21EZ, UK (fax: +44 1223 336 033; E-mail address: deposit@ccdc. cam.ac.U.K).

2.5 Preparation of photoelectrodes (ZnO nanograins and TiO_2 nanorod arrays)

2.5.1 Formation of ZnO compact layer on FTO

The fluorine-doped tin oxide (FTO) having a resistance 16 Ω/□ (ohms per square) was cleaned with a soap solution, followed by 15 min ultrasonication in a mixture of double-distilled water (DDW), ethanol and then again washed with a copious amount of DDW.[38,39] Further, a ZnO compact layer on the FTO substrate was deposited using the SILAR method. Typical SILAR process includes 0.1M $Zn(NO_3)_2.6H_2O$ solution in DDW and 20% ammonia solution in one beaker; the second beaker contains the cold water and the third beaker filled with hot water (80°C). During the SILAR process, FTO was dipped in the successive beaker with 5 sec, 2 sec, and 10 sec, respectively. After thirty cycles, ZnO compact layer was formed on the FTO substrate. Finally, the films were annealed in the box furnace at 450°C for 1 h.

2.5.2 Developments of ZnO photoelectrodes and AMT, AET photosensitization

In the second step, after the ZnO compact layer was formed on the FTO substrate, the ZnO paste was prepared separately using thoroughly grinding of 0.5 g ZnO powder with 10 ml ethanol in mortar and pestle. The mixture was ultrasonicated for 1 h. Furthermore, ethylcellulose and 1.36 g of α-terpineol were added, followed by 4 h ultrasonication. Again, 2-3 drops of acetylacetone were added to the above-prepared mixture and then ultrasonicated for the next 1 h. Afterward, the mixture was filled in a bottle and was kept in an incubator for 9 h to form the paste. Finally, the doctor blade method was used to prepare ZnO nanograin photoanodes. In the typical process,

two edges of the compact layered FTO covered by scotch tape and ZnO nanograin paste was coated on a compact ZnO layered FTO substrate. The as-deposited film was air-dried at 60°C in an incubator for 3 h, and then finally annealed in the box furnace at 450°C for 1 h. Lastly, to increase the photoanode's porosity, the ZnO nanograin photoelectrodes were treated with water vapors[40] using a steamer. After water vapors treatment, the photoelectrodes were dried at room temperature (27°C) and annealed at 120°C in a furnace for 1 h. The AMT, AET photosensitized ZnO photoelectrodes were prepared via the sensitizing process. The 0.01 M solution of photosensitizers in methanol was prepared first. Then, doctor-bladed ZnO nanograin photoanodes were dipped into the sensitizer solution for 72 h at room temperature (27°C) under the dark condition. After loading photosensitizers, the photoanodes were washed with ethanol for 10 s to remove the unloaded and loosely attached photosensitizer molecules. Finally, these AMT, AET photosensitized ZnO photoelectrodes were termed ZnO/AMT and ZnO/AET.

2.5.3 Developments of TiO_2 nanorod photoelectrodes and AMT, AET photosensitization

The FTO was cleaned and having a resistance of 16 Ω/□ (ohms per square). Synthesis of TiO_2 nanorod (TiO_2NR) by hydrothermal process, a 1 ml of titanium butoxide was added in the 30 ml of concentrated HCl stirred for 5 min. The same amount of DDW (30 ml) was poured into the above solution with vigorous stirring for the next 30 min. Further, this solution was transferred into the Teflon-lined stainless-steel autoclave. Afterward, two FTO's were fitted into the FTO holder and kept into the autoclave such that its conducting edges are facing the walls of the autoclave. Finally, the autoclave was closed and maintained at 150 °C for 4 h in the electric oven. After cooling to room temperature, the white TiO_2/ FTO films were washed with a copious amount of DDW and dried at room temperature (27 °C).[41,42] The AMT, AET photosensitized TiO_2NR photoelectrodes were prepared via the sensitizing process. Initially, a 0.01 M solution of photosensitizers (AMT and AET) in methanol was prepared separately. Then, hydrothermally prepared TiO_2NR photoanodes were dipped into the sensitizer solution for 72 h at room temperature (27°C) under the dark condition. After loading photosensitizers, the photoanodes were washed with ethanol for 10 s to remove the unloaded and loosely attached photosensitizer molecules. Finally, these AMT, AET photosensitized TiO_2NR photoelectrodes were denoted TiO_2NR /AMT and TiO_2NR /AET.

2.6 Construction of dye-sensitized solar cell (DSSC)

In the present investigation, DSSC is fabricated with the key parameters such as AET and AMT sensitized ZnO nanograin and TiO_2 nanorod based working electrodes, redox-mediator (electrolyte), and a counter electrode. The spacer was used (thickness ~40 μm) between the working electrode and counter electrode with a 0.5 x 0.5 cm^2 active cell area. The platinum electrode was used as a counter electrode. The photosensitizers loaded photoanodes were sandwiched with a platinum electrode. The polyiodide was injected between the photoelectrode and platinum electrode; simultaneously, care was taken to avoid any air bubble inside the solar cell assembly. Electrolyte solution was a mixture of 0.5M tetra-*n*-propylammonium iodide ($(CH_3CH_2CH_2)_4NI$) and 0.05M iodine (I_2) in an (ethylene carbonate: acetonitrile) mixed solvent (80: 20) proportion was used.[43] This prepared device was further used for the photovoltaic measurement. The components and the experimental Scheme of AET and AMT photosensitized ZnO and TiO_2 based DSSC is shown in Fig. 2.

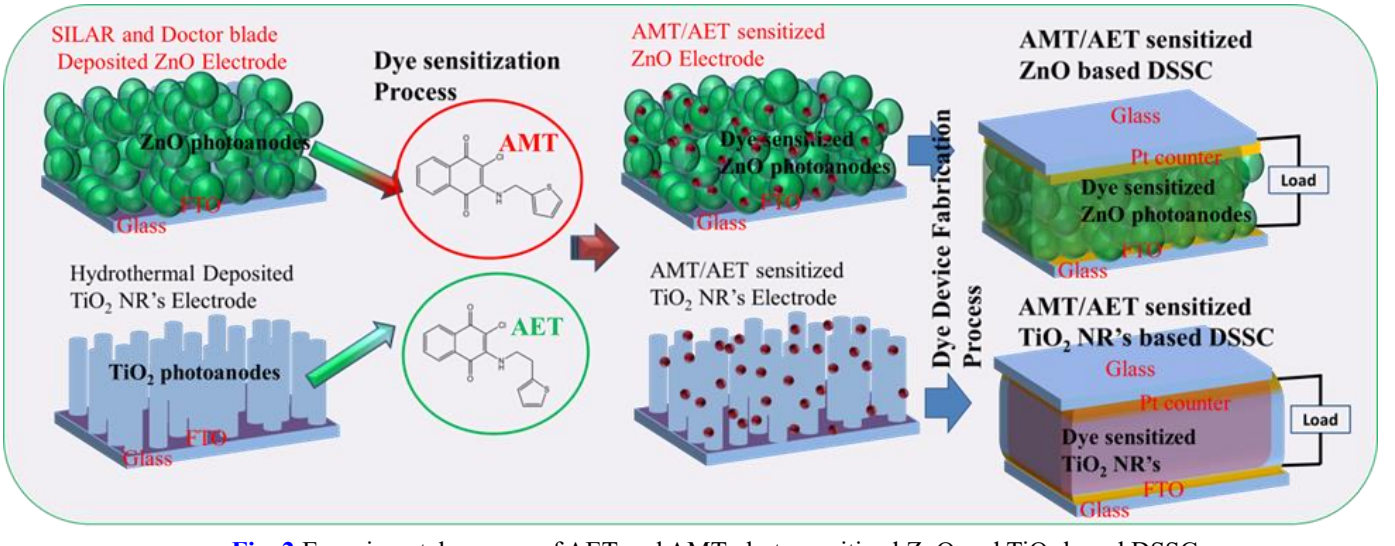

Fig. 2 Experimental process of AET and AMT photosensitized ZnO and TiO_2 based DSSC.

2.7 Characterization of photosensitizers

2.7.1 Characterization of AMT

Orange solid, Yield: 0.78 g, 90.51 %. mp: 125.02°C (Fig. S3 in ESI†). Anal. data calc. for $C_{15}H_{10}O_2NSCl$ (303.7 g/mol): C, 59.31; H, 3.32; N, 4.61 %. Found: C, 59.22; H, 3.04; N, 4.06%. FT-IR (ATR, cm^{-1}): 3316, 1671, 1595, 1566, 1512, 1333, 1290, 1242, 1137, 1056, 1017, 829, 716, 702, 627, 546, 501, 449 (Fig.S1 in ESI†). ^{1}H NMR (400 MHz, DMSO-d_6, δ(ppm)): 8.08 (d, J = 7.5 Hz, 1H, Ar), 7.95 (d, J = 7.5, 1H Ar), 7.81(t, J = 7.5 Hz,1H, Ar), 7.73(t, J = 8 Hz, 1H, Ar), 7.40 (t, J = 5Hz, 1H, Ar), 7.04 (d, J = 7.5 Hz, 1H Ar), 6.97 (d, J = 6 Hz 1H), 5.11 (s, -CH_2), 2.51(s, -NH) (Fig. S5 in ESI†).^{13}C NMR (100 MHz, DMSO-d_6, δ(ppm)):180.60, 176.33, 176.04, 142.90, 142.84, 135.41, 135.14, 133.34, 132.17, 131.37, 130.38, 127.54, 127.31, 127.01, 126.31, 126.07, 125.76, 42.77, 40.53, 40.32, 40.11, 39.91, 39.70, 39.49, 39.28 (Fig. S6 in ESI†). LC-MS (m/z): 303.76 g/mol (303.70 g/mol) (Fig. S9 in ESI†).

2.7.2 Characterization of AET

Orange solid, Yield: 0.78 g, 90.51 %. mp: 120.28 °C (Fig. S4 in ESI†). Anal. data calc. for $C_{16}H_{12}O_2NSCl$ (317.7 g/mol): C, 60.47; H, 3.81; N, 4.41 %. Found: C, 60.22; H; 3.78, N, 4.50%.FT-IR (ATR, cm^{-1}): 3269, 1674, 1645, 1601, 1572, 1503, 1443, 1357, 1332, 1290, 1264, 1247, 1227, 1132, 1069, 820, 787, 719, 677, 610, 548, 497, 465, 415 (Fig. S2 in ESI†). ^{1}H NMR (400 MHz, DMSO-d_6, δ(ppm)):7.98 (d, J = 7.5 Hz, 1H, Ar), 7.96 (d, J = 7.5, 1H Ar), 7.82(t, J = 7.5 Hz, 1H,Ar), 7.74(t, J = 8 Hz, 1H, Ar), 7.52 (t, J = 5 Hz, 1H, Ar), 7.33 (d, J = 7.5 Hz, 1H, Ar), 6.94 (t, J = 5 Hz 1H), 3.99 (q, J = 6 Hz, 2H-CH_2), 3.14 (t, J = 6 Hz, 2H, -CH_2), 2.51(s, -NH) (Fig. S7 in ESI†).^{13}C NMR (100 MHz, DMSO-d_6, δ(ppm)):180.57, 175.92, 145.65, 140.85, 135.40, 133.19, 132.33, 130.32, 129.73, 127.55, 126.95, 126.29, 126.01, 124.84, 45.89, 31.43 (Fig. S8 in ESI†). LC-MS (m/z): 317.9 g/mol (317.75 g/mol) (Fig. S10 in ESI†).

2.8 Characterization of ZnO nanograin and TiO_2 nanorods arrays photoelectrodes

The structure and crystallite size of prepared ZnO nanograin and TiO_2 nanorods arrays based photoelectrodes was calculated using a powder X-ray diffractometer, Bruker D8, with Cu-kα radiation source, wavelength (λ) = 0.154 nm and the angular range of 20-80º. The X-ray tube used with a fixed current of 30 mA and voltage set 40 kV, respectively. The UV-Vis absorption spectra of dyes and photoanodes were collected using the Jasco Ultraviolet-Visible spectrophotometer model (V-670). The morphology of photoanodes was further analyzed using the JEM-2010 field emission-scanning electron microscopy (FE-SEM) instrument (SUPRA40VP, Germany). The Fourier-transform infrared spectroscopy (FT-IR) spectra of photosensitizers (AET and AMT) and photosensitizers loaded photoanodes were recorded in 4000-400 cm^{-1} using a BRUKER FT-IR spectrophotometer.

2.9 Photovoltaic measurements

The photocurrent density-voltage (J-V) characteristic curves of DSSC's were obtained for an active cell area (0.25 cm^2) generated using a Keithley 2400 source meter and solar simulator (ENLITECH Model SS-F5-3A) with incident light intensity 100 mW cm^{-2}. Electrochemical impedance spectroscopy (EIS) was measured using potentiostat/galvanostat (Vertex IVIUM Technologies, Netherlands). Measurements were carried out at applied potential -0.22 V with 0.01 V amplitude over a frequency range of 1 Hz – 1000 kHz under illumination with a light intensity of 100 mW cm^{-2}. All the EIS spectra were fitted using ZView software.

3. Result and discussion

3.1 Synthesis and characterization of photosensitizer AMT and AET

Photosensitizer AMT and AET were synthesized (Scheme1a, b) at room temperature (26°C) and characterized by FT-IR (Fig. S1 and S2 in ESI†), ^{1}H (Fig. S5 and S7 in ESI†) and ^{13}C (Fig. S6 and S8 in ESI†) NMR, elemental analysis, LC-MS (Fig. S9 and S10 in ESI†), UV-visible spectroscopy, and single-crystal X-ray diffraction studies. The melting point of photosensitizers was obtained by Differential Scanning Calorimetry (DSC) (Fig. S3 and S4 in ESI†). A sharp peaks at ~3316 cm^{-1}, 1671 cm^{-1}, 1595 cm^{-1} and 1565 cm^{-1} in FT-IR were assigned to ν_{N-H}, $\nu_{C=O}$, ν_{C-N}, $\nu_{C=C}$ vibrations respectively. The characteristics paranaphthoquinone (p-NQ) vibrations were observed at~ 1290 cm^{-1} and 1242 cm^{-1}, while $\nu_{C(3)-Cl}$ was observed at 716 cm^{-1} for AMT.[30,44] For AET, a sharp peak at 3269 cm^{-1}, 1674 cm^{-1}, 1601 cm^{-1} and 1572 cm^{-1} in FT-IR were assigned to ν_{N-H}, $\nu_{C=O}$, ν_{C-N}, $\nu_{C=C}$ vibrational frequencies, respectively. A characteristics paranaphthoquinone vibrations were observed at ~ 1290 cm^{-1} and 1247 cm^{-1}, while $\nu_{C(3)-Cl}$ was observed at 719 cm^{-1} for AET.[30,44]

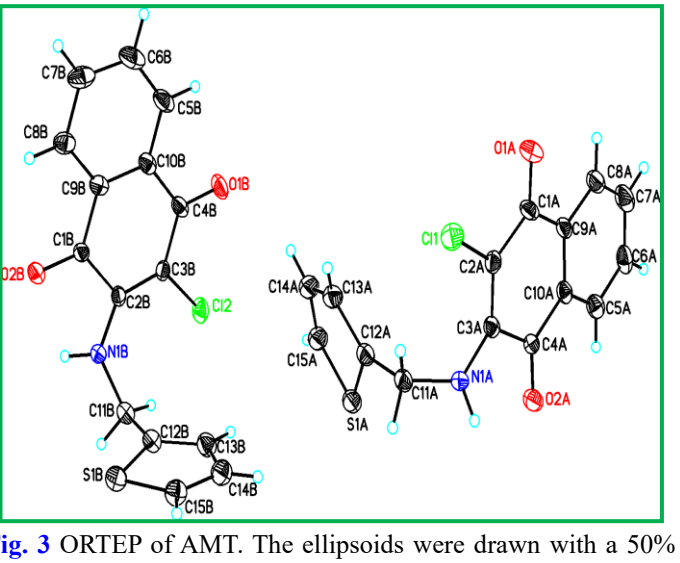

Fig. 3 ORTEP of AMT. The ellipsoids were drawn with a 50% probability.

3.2 Single-crystal X-ray diffraction studies of AMT photosensitizer

Fig. 3 shows ORTEP (Oak Ridge Thermal Ellipsoid Plot) of AMT photosensitizer, and the ellipsoids were drawn with a 50% probability. Besides, Fig. 4 shows π-π stacked dimer chains of the asymmetric molecules of AMT. The crystal data of AMT and hydrogen bonding geometries are presented in Table S1 and Table S2 in ESI†, respectively. AMT crystallizes in monoclinic space group *P2/c*. The asymmetric unit comprises two AMT molecules; those differed in bond distances (Fig. S11 in ESI†) and hydrogen bonding interactions (Table S2 in ESI†). The carbonyl bond distances are C(1)-O(1A) = 1.227 Å, C(1B)-O(2B) = 1.217 Å and C(4A)-O(2A) = 1.221Å. These distances were similar to the oxidized form of similar naphthoquinones.[28,29,45,46,47] Also, the bond angles of ∠C (3A)-N(1A)-C(11A) and ∠C(2B)-N(1B)-C(11B) are found to be 127.81°. The naphthoquinone and thiophene rings are not on the plane. The planes of the naphthoquinone ring and thiophene rings of the asymmetric molecules make an angle of 85.2° and 82.4°. One of the asymmetric molecules is in the vicinity of four neighboring molecules, while the other in the vicinity of three similar molecules (Fig.S12 in ESI†). With the opposite orientation of the molecules, both the molecules of asymmetric unit form a dimer via N-H···O interaction, that supported by C···S close contacts. Further, a polymeric chain of the π-π stacked dimer is formed via C-H···O interaction (Fig.4).

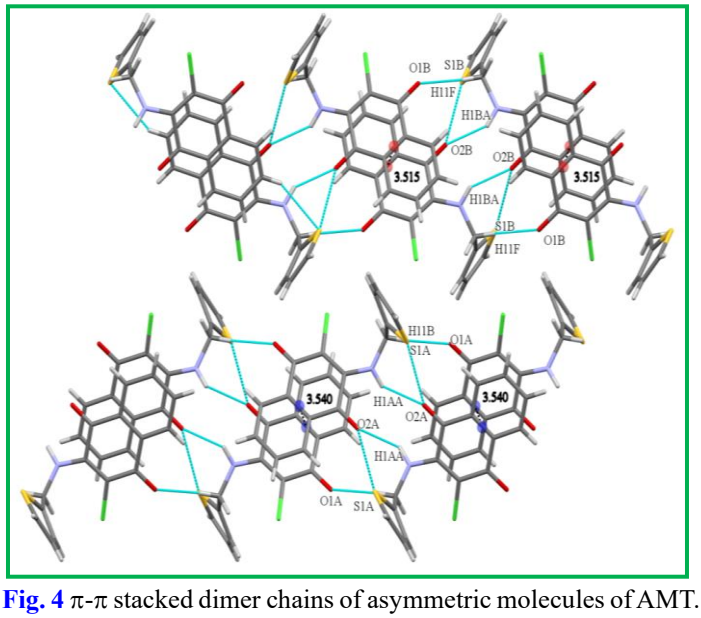

Fig. 4 π-π stacked dimer chains of asymmetric molecules of AMT.

3.3 Surface morphology of ZnO and TiO_2NR photoanodes

Surface and cross-sectional FESEM of ZnO nanograin paste on FTO revealed that the FTO's entire surface is covered with hexagonal and oval-shaped ZnO nanograins as shown in Fig. 5(a). The cross-sectional FESEM of the ZnO photoanode shows a thickness of the ZnO nanograin based photoanode is 11.95 µm Fig. 5(b). It can also be seen that the ZnO nanoparticles covered on the FTO show the porous structure of the developed photoanode. The porous structure of the photoelectrode allows efficient dye loading for effective DSSCs. Despite the ZnO electrode, the Fig. 5(c) and Fig. 5(d) shows the surface and cross-section images of the hydrothermally deposited TiO_2 photoelectrode. Fig. 5(d) shows the thickness of TiO_2 nanorods is approximately 1.7 µm. The vertically aligned TiO_2 nanorod arrays uniformly covered the FTO conducting side. The nanorod's upper faces are round-shaped, and some space is present in between the two nanorods led to a porous structure to hydrothermally TiO_2 photoelectrodes. This porous structure could be helpful during the photosensitizer loading and photovoltaic measurements. The more electrolyte is inserted into porous and more give rise to the more active surface area.[48]

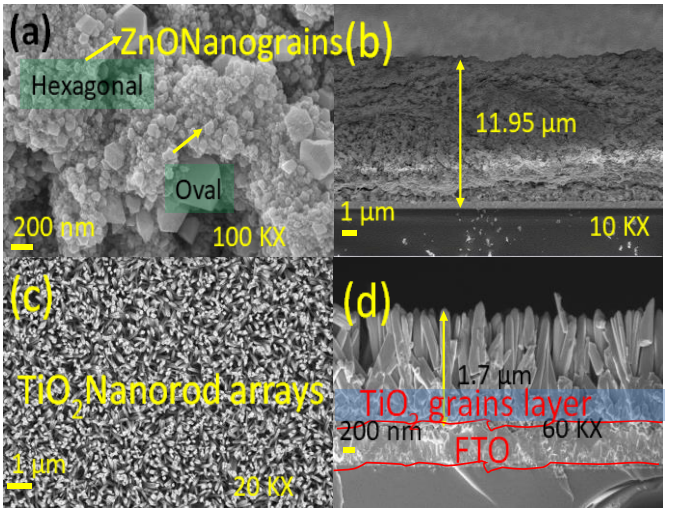

Fig.5 Surface and cross-sectional FE-SEM images of (a, b) doctor bladed ZnO nanograin photoanodes, (c, d) hydrothermally based TiO_2 nanorod arrays grown on FTO surface.

3.4 X-ray diffraction analysis of ZnO and TiO_2NR Photoanodes

Fig. 6(a) depicts the XRD patterns of doctor bladed ZnO nanograins photoelectrodes.The XRD peaks observed at 2θ = 31.6, 34.3, 36.1, 47.3, 56. 4, 62.7 and 68.3 correspond to (100), (002), (101), (102), (110), (212), and (201) planes of hexagonal structure of ZnO (JCPDS file 36-1451 of ZnO). The high-intensity peaks in the XRD pattern of doctor-bladed ZnO nanograins photoelectrodes indicate ZnO nanoparticle's polycrystalline nature.[49] The FTO substrate peaks are indicated by "*". Further, Fig. 6(c) depicts the XRD pattern of the hydrothermally deposited TiO_2 nanorod arrays grown on the FTO substrate at 150 ºC for 4h. The presence of XRD diffraction peaks at 2θ = 36.13°, 41.2°, and 54.31° have resembled the tetragonal phase of the rutile TiO_2 (reference code. 98-002-4277). The results well agreed with the results obtained by Wu *et al.*.[50] Furthermore, Fig.6. (b,d) shows the full-width half maxima (FWHM) of (100) and (101) peaks of the ZnO and TiO_2NRs. The crystallite size of ZnO and TiO_2NR at (100) and (101) peaks is calculated by using Scherrer's formula.[51] The crystallite size of ZnO is 13.51 nm

and 24.26 nm for TiO_2NR, respectively. However, the higher intensity of FTO peaks in the TiO_2NR/FTO photoanodes is due to the ZnO-based photoanodes lower thickness. The results are well matched to the FESEM.[52]

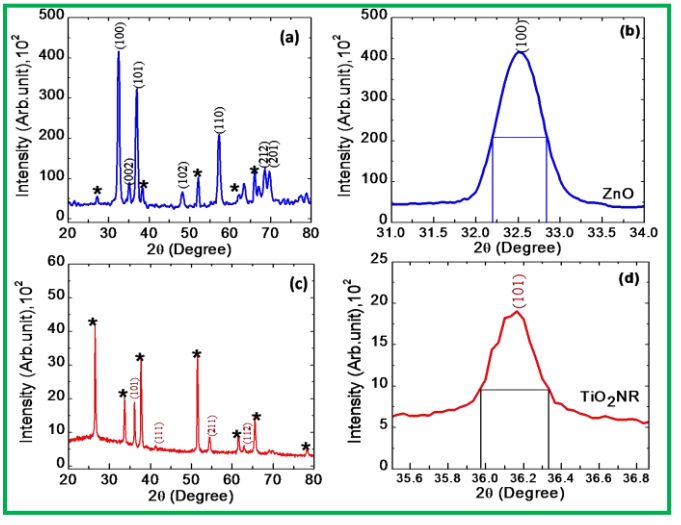

Fig. 6 a) XRD patterns of Doctor bladed ZnO nanograins photoelectrodes, (b) Full-width half maxima (FWHM) peak for crystallite size analysis of ZnO (c) hydrothermally deposited TiO_2 nanorod arrays grown on FTO substrate. (FTO peaks indicated by "*") and (d) FWHM peak for crystallite size analysis of TiO_2NR.

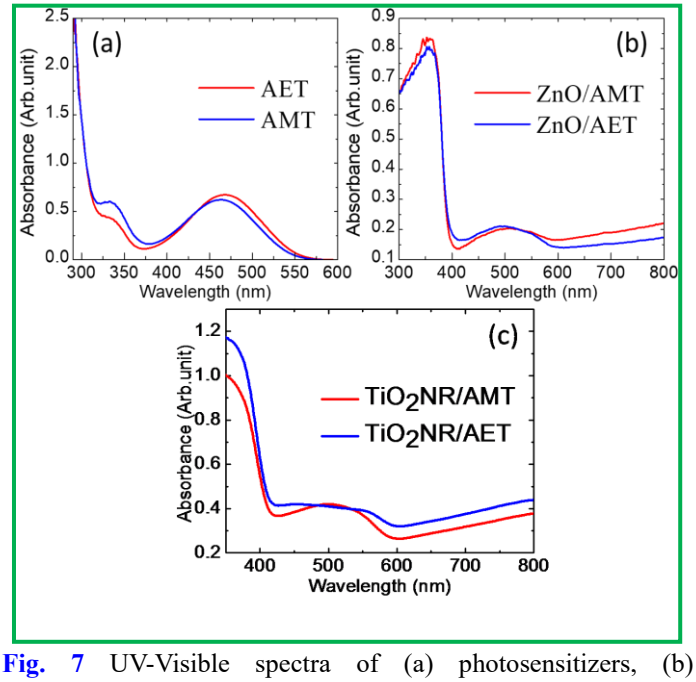

Fig. 7 UV-Visible spectra of (a) photosensitizers, (b) Photosensitizers loaded ZnO photoanodes, and (c) Photosensitizers loaded TiO_2NR photoanodes.

3.5 UV-Vis absorption analysis of photosensitizers (AMT, AET) and Photoanodes (ZnO/AMT, ZnO/AET, TiO_2NR/AMT, and TiO_2NR/AET)

UV-Visible spectra of photosensitizers and photosensitizer loaded photoanodes ZnO/AMT, ZnO/AET, TiO_2NR/AMT and TiO_2NR/AET are shown in Fig. 7(a,b,c). Bathohromic shift observed in the photosensitizers loaded on the photoanode is shown in Table S9 in ESI†. UV- vis spectra of photosensitizer's AMT and AET is shown in Fig. 7(a). The maximum absorption wavelength (λ_{max}) at ~464 nm and 469 nm, respectively, for AMT and AET. The photosensitizer's UV-vis spectra loaded photoanodes (ZnO/AMT, ZnO/AET) are shown in Fig. 7(b). The maximum absorption wavelength (λ_{max}) at 503 nm and 500 nm, respectively ($n \rightarrow \pi^*$ electronic transition). The UV-vis spectra of photosensitizer's loaded photoanodes (TiO_2NR/AMT, TiO_2NR/AET) are shown in Fig. 7(c). The maximum absorption wavelengths (λ_{max}) of TiO_2NR/AMT, TiO_2NR/AET at 506 nm and 508 nm ($n \rightarrow \pi^*$) electronic transition.

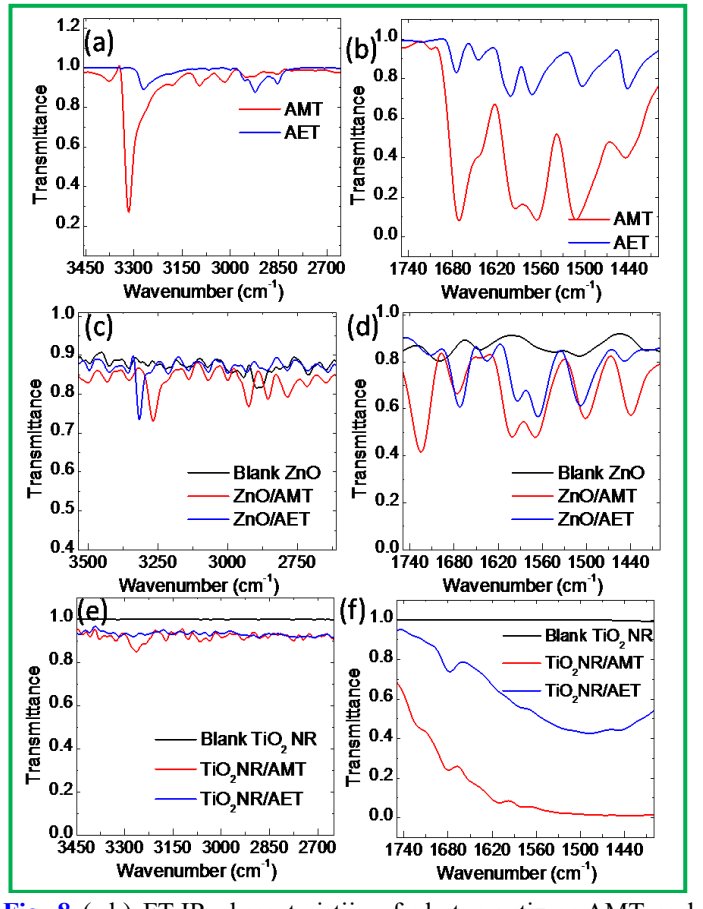

Fig. 8 (a,b) FT-IR characteristiic of photosenstizers AMT and AET, (c,d) FT-IR of ZnO photoanodes and (e,f) FT-IR of TiO_2 photoanodes.

3.6 FT-IR analysis of photosensitizers and photoanodes

Fig. 8(a,b) showed the FT-IR spectra of thionaphthoquinone photosensitizers (AMT, AET), and Fig. 8(c-f) of ZnO, TiO_2NR photoanodes measured in the range of 3450-2650 cm^{-1} and 1750-1400 cm^{-1}, respectively. The FT-IR band frequencies of all photosensitizers and photoanodes are summarized in Table 1. The ν_{N-H} band of photosensitizers AMT (3316 cm^{-1}) and AET (3269 cm^{-1}) was decreased by 50 cm^{-1} and increased by 48 cm^{-1}in their ZnO photoanodes, respectively. Whereas as it was decreased by 54 cm^{-1} and increased by 4 cm^{-1} in the TiO_2NR photoanodes. On the other hand, the $\nu_{C=O}$ frequencies of photosensitizers observed at 1671 (AMT) and 1674 cm^{-1}

(AET) shifted to higher wavenumber by 4 cm^{-1} and lower wavenumber 2 cm^{-1} (in ZnO) and higher wavenumber (Bathochromic shift) by 5, 6 cm^{-1} respectively (in TiO_2NR) for their photoanodes. However, the ν_{C-N} frequency observed at 1595 cm^{-1} (AMT) and 1601 cm^{-1} (AET), is increased by 7 cm^{-1} and decreased by 7 cm^{-1} respectively (in ZnO) and bathochromic shifted to 15 cm^{-1}, 10 cm^{-1} respectively (in TiO_2NR) photoanodes.

Table 1 FT-IR band frequencies of all photosensitizers and photoanodes.

Photosensitizers/ Photoanode	ν_{N-H} band frequencies (cm^{-1})	$\nu_{C=O}$ band frequencies (cm^{-1})	ν_{C-N} band frequencies (cm^{-1})
AMT	3316	1671	1595
ZnO/AMT	3266	1675	1602
TiO_2NR/AMT	3262	1677	1610
AET	3269	1674	1601
ZnO/AET	3317	1672	1594
TiO_2NR/AET	3273	1679	1611

Table 2 Comparative photovoltaic performance of ZnO nanograin and TiO_2 nanorod photoanodes DSSCs.

Photosensitizers/ Samples	V_{oc} (V)	Fill factor	J_{sc} (mA/cm^2)	Efficiency η (%)
ZnO/AMT	0.21	60	0.17	0.02
ZnO/AET	0.22	59	0.22	0.03
TiO_2NR/AMT	0.41	33	1.73	0.23
TiO_2NR/AET	0.42	44	1.73	0.32

3.7 Photovoltaic performance

3.7.1 J-V characterization of ZnO/AMT and ZnO/AET photoanodes

The DSSCs properties of the ZnO electrode-based DSSC were investigated in detail. The prepared ZnO/AMT and ZnO/AET electrodes were used as photoanodes, and the platinum-coated FTO substrate was utilized as a counter electrode in the DSSC application. The fabrication scheme of ZnO/AMT and ZnO/AET based DSSC is shown in Fig. 9(a), and the data presented in Table 2. Fig. 9(b) illustrates that ZnO/AMT based DSSC exhibits short-circuit current density (J_{sc}) of 0.17 mA·cm^{-2}, open-circuit voltage (V_{oc}) of 0.21V, fill factor (*FF*) of 0.60%, and a power conversion efficiency (PCE) of 0.02%. Interestingly, except for fill factor (*FF*) of 0.59%, a ZnO/AET based DSSC exhibits the higher short-circuit current density (J_{sc}) of 0.22 mA·cm^{-2}, open-circuit voltage (V_{oc}) of 0.22V, and a power conversion efficiency (PCE) of 0.03% than that of the ZnO/AMT based DSSC.

3.7.2 Electrochemical impedance spectroscopy (EIS) analysis of ZnO/AMT and ZnO/AET photoanodes

Furthermore, to investigate the kinetics and energetics of charge transport and recombination in DSSCs, the electrochemical impedance spectroscopy (EIS) has been used. Fig. 9(c) shows the electrochemical impedance spectra of the ZnO/AMT and ZnO/AET based DSSC under dark conditions. The EIS data were fitted by ZView software using the equivalent circuit (Inset of Fig. 9(c)), and the fitted values are listed in Table 3. The equivalent circuit consists of Two resistance and corresponding capacitance. Rs is the resistance between the FTO and ZnO nanograins interface through the non-zero intercepts on the real axis of the plot between Z,' and Z", and the parallel resistance R1 is the bulk charge-transfer resistance, and CPE1 denotes corresponding double-layer capacitance; meanwhile, R2 and CPE2 characterize the charge-transport resistance and the double-layer capacitance between of ZnO nanograin based photoanodes and the electrolyte interface, respectively.[53,54] It was reported that under dark conditions, the more considerable value of R2 leads to the reduction in charge recombination rate, which is favorable towards the enhancement in device efficiency.[55] The schematic of charge transfer in ZnO nanograin based DSSC is shown in Fig. 9(d). The Bode phase plot shows the signature peak, representing interfacial electron recombination towards the low-frequency region for the ZnO/AMT and ZnO/AET based DSSCs (Fig. 9(e)). Electron lifetime was calculated from the bode plot using formula $\tau_{eff} = 1/2\pi f$.[54] The considerable increase in the τ_{eff} values of ZnO/AET than the ZnO/AMT indicates the effective suppression of the back reaction between the photogenerated electrons. This may be the possible reason for the higher power conversion efficiency of ZnO/AET based DSSC than that of the ZnO/AMT photoanode-based DSSC.[56] Further, the photovoltaic properties of ZnO/AET and ZnO/AMT based DSSC under one sunlight condition were characterized, with the parameters summarized in Table 3.

Table 3 Electron Transport Properties of the photoanodes by using ZnO based DSSCs.

Samples/ DSSC parameters	R_1 (Ω)	R_2 (Ω)	R_2/R_1	Frequency (Hz)	η_{CC}	τ_{eff} (m Sec)	L_n	τ_D (m Sec)	D_{eff} (m sec^{-1})	L_{eff} (mm)
ZnO/AMT	273.7	6983	25.51	20.89	0.96	7.6	5.05	0.298	0.4758	0.0601
ZnO/AET	201.1	8877	44.14	12.02	0.97	13.24	6.64	0.299	0.4778	0.0795

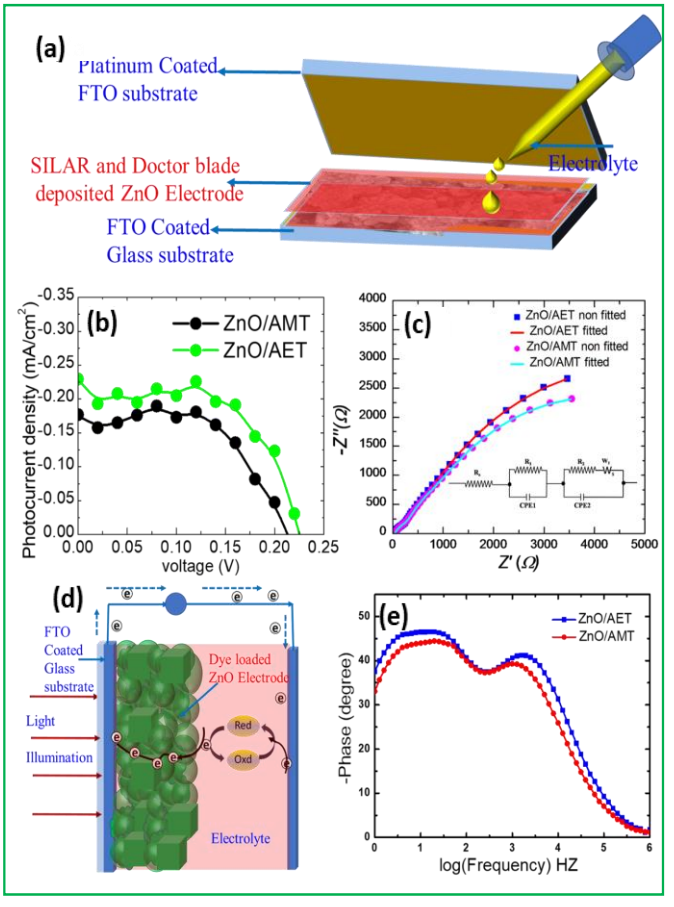

Fig. 9 (a) Schematic representation of fabricated DSSC based on ZnO electrode, (b) J-V, (c) Nyquist plot (Inset reveals the Equivalent circuit model for EIS analysis), (d) corresponding Scheme of a DSSC formation with marked electron flow and (e) Bode phase plot of fabricated AET and AMT loaded ZnO electrode DSSCs.

3.7.3 J-V characterization of TiO_2NR/AMT and TiO_2NR/AET photoanodes

To evaluate the effect of surface morphology on the photovoltaic properties of DSSC, the TiO_2/AET and TiO_2/AMT based DSSC devices were fabricated and compared with the ZnO nanograin based DSSC (ZnO/AET and ZnO/AMT) under the same conditions. Fig. 10(a) shows the *J–V* characteristics for the AET and AMT loaded TiO_2 electrode-based DSSCs. The modified TiO_2NR/AET photoanode exhibits a short circuit current density (J_{sc}) of 1.73 mA cm^{-2}, an open-circuit voltage (V_{oc}) of 0.42 V, and a fill factor (*FF*) of 0.44, resulting in the power conversion efficiency (η) of 0.32%. Thus, compared with ZnO/AMT, ZnO/AET, and TiO_2/AMT, respectively, were significantly improved in TiO_2NR/AET.

The improved photocurrent efficiency (PCE) of the AET loaded photoanodes than the AMT photosensitizer is because of the photosensitizer AET's different substituents than the AMT oxidation. Thus, the photosensitizer structure and the substituents are affecting the efficiency of DSSCs.[57] Previous studies also reported the effect of different substituents like alkyl chains, alkoxy groups, aryl groups, anthracene & naphthalene rings on the efficiency of DSSCs.[58-61] More recently, Khanmohammadi *et al*. also reported the electron-donating groups on the moiety part of the naphthoquinone photosensitizers to increase the donor part's electron density photosensitizers.[62] Therefore, in the present study, the effect of the electron-donating substituent such as –CH_2– led to an increase in the efficiency of the AET photosensitizer loaded ZnO and TiO_2NR photoanodes. ZnO nanograins' power conversion efficiency is much lower than TiO_2NR because the morphology of the TiO_2NR is more porous than the ZnO nanograin photoanode. As a result of the higher surface area, to increase the number of dye molecules are adsorbed onto the TiO_2NR photoelectrode.[63] Due to this reason, the absorption of sunlight is increased and increases its efficiency.

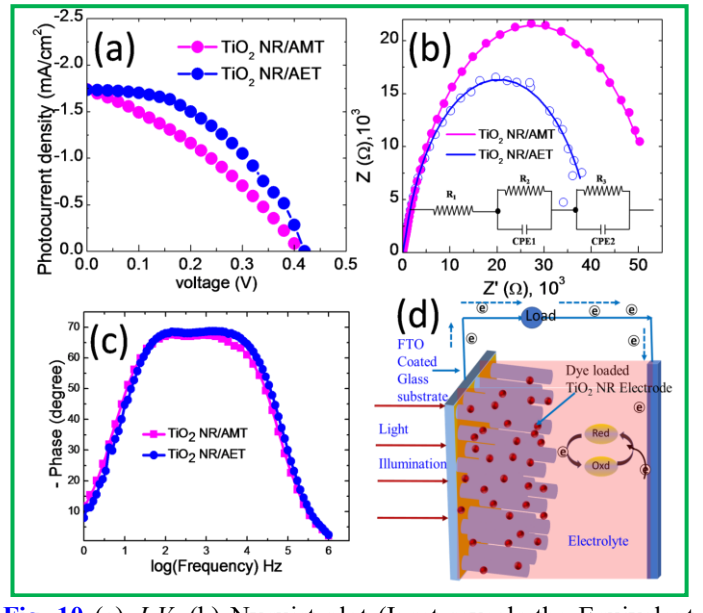

Fig. 10 (a) *J-V*, (b) Nyquist plot (Inset reveals the Equivalent circuit model for EIS analysis), (c) Bode phase plot of fabricated AET, and AMT loaded TiO_2 electrode DSSCs and (d) corresponding Scheme of a DSSC with marked electron flow.

3.7.4 Electrochemical impedance spectroscopy (EIS) analysis of TiO_2NR/AMT and TiO_2NR/AET photoanodes

The corresponding electron transport/recombination dynamics in the TiO_2NR network, electron transfer between the counter electrode and electrolyte under dark conditions were carried out using EIS. The EIS data were fitted using ZView software to determine the electrochemical parameters, and fitted data are presented in Table 4. The R2 value of the TiO_2NR/AET is a bit smaller than that of the TiO_2NR/AMT, suggesting the one more opportunity for electron loss while traveling to FTO. However, the TiO_2NR/AET leading to significantly improved photovoltaic properties than that of the TiO_2NR/AMT DSSCs. The results indicated that rather than the electrical contact between the photosensitizer loaded TiO_2NR, the significant AET dye loading, light absorption, and scattering by TiO_2 NR/AET photoanodes are the main factors resulting in the highest J_{sc} and maximum η. Fig. 10(c) displays the Bode plot

Table 4 Electron transport properties of the photoanodes by using TiO_2NR based DSSCs.

Samples/ DSSC parameters	R_1 (Ω)	R_2 (Ω)	R_2/R_1	Frequency (Hz)	η_{cc}	τ_{eff} (m sec)	L_n	τ_D (m sec)	D_{eff} (m sec^{-1})	L_{eff} (mm)
TiO_2NR/AMT	352.8	54451	154.33	13.33	0.99	1.10	12.4	0.007	0.405	0.0211
TiO_2NR/AET	324.3	40164	123.84	13.28	0.99	1.18	11.1	0.009	0.303	0.0189

obtained from EIS analyses. The actual lifetime (τ_{eff}) of the electrons at the interface between the counter electrode and electrolyte can be calculated according to the literature, and the value is given in Table 2.[64,65] The comparative photovoltaic performance of ZnO nanograin and TiO_2 nanorod photoanodes DSSCs are summarized in Table 2. The architecture of AET and AMT dye-sensitized solar cells based on TiO_2NR photoanodes is shown in Fig. 10(d).

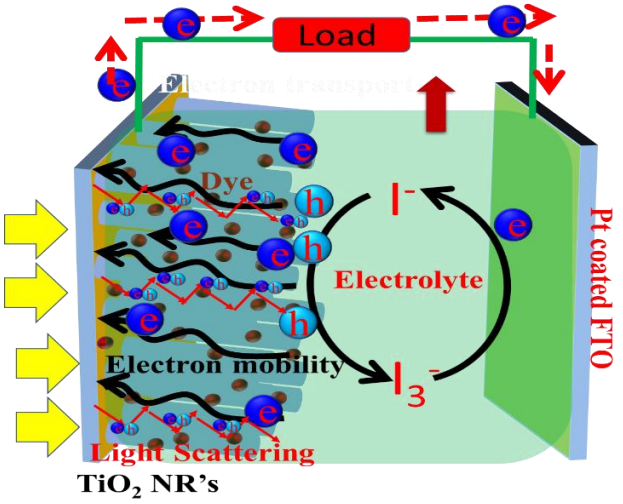

Fig. 11 Schematic diagram of the light scattering effects in the TiO_2NR's based DSSC.

In the present investigation, a schematic of a DSSC is shown in Fig. 11. The central part is AET sensitized TiO_2NR's photoelectrode, electrolyte solution, and thin catalyst layer of Platinum (Pt) was deposited - on the counter electrode.[66] The TiO_2NR increased the dye loading capacity and improved light scattering ability due to high surface-area-to-volume ratio and porous nanostructure.[67, 68] Under the light illumination, due to TiO_2 nanorods structure exhibits significant light scattering. The effective light scattering layer is essential to reduce light loss during the DSSC process, reducing power conversion efficiency (PCE).[69] Therefore, corresponding to the energy difference between its highest occupied molecular orbital (HOMO) and lowest unoccupied molecular orbital (LUMO), the AET dye-sensitized on the surface of TiO_2nanorod absorbs more the incident photon flux and excited from the ground state (S) to the excited state (S*).[70]

Further, the excited state of the dye molecule (S*) injects the electron into the conduction band (CB) of TiO_2NR.[71] Subsequently, the electron flows through the one-dimensional TiO_2NR's nanostructure to the load before the counter electrode entrance. Such an effective electron transfer in nanorod structures can retard the fast electrons–holes recombination on TiO_2NR's.[72] These electrons are further used to reduce the oxidized redox mediator on the counter electrodes surface. Thus, the electron transfer cycle will be completed when the oxidized AET dye molecule is facilitated to its ground state by the redox mediator in the electrolyte in the following ways: the oxidized AET photosensitizer is reduced by I^- ions in the electrolyte, regenerating the ground state of the sensitizer, and I^- ions are oxidized to I_3^- ions and the I^- ions were regenerated on the counter electrode surface by interacting electrons with I_3^- ions.[73] Thus, all the above merits of TiO_2 nanorods based photoanodes improved the performance and stability of DSSCs.

4. Conclusions

We have successfully fabricated and compared the ZnO nanograin and TiO_2 nanorod based dye-sensitized solar cells (ZnO/AMT, ZnO/AET, TiO_2-NR/AMT, TiO_2-NR/AET) using thionaphthoquinones photosensitizers, viz; AMT; 2-((thiophen-2-yl)methylamino)-3-chloro-naphthalene-1,4-dione, AET; 2-((thiophen-2-yl)ethylamino)-3-chloro-naphthalene-1,4-dione are synthesized from 2,3-dichloronaphthalene-1,4-dione. This development builds on our successful synthesis of thionaphthoquinones photosensitizers, highly crystalline TiO_2NR, and the ability to agglutinate the AMT, AET with nanostructured TiO_2NRs. The FE-SEM and optical properties confirm the fabricated TiO_2NR based photoanode provides an appropriate charge transport, pore structure, and significant light scattering effect than that of the ZnO nanograin photoanodes. The AMT and AET photosensitized ZnO nanograins and hydrothermally synthesized TiO_2NR electrodes based on DSSC's exhibited power conversion efficiencies of 0.02 (ZnO/AMT), 0.03 (ZnO/AET), 0.23 (TiO_2NR/AMT), and 0.32% (TiO_2NR/AET), respectively. The electron-donating substituent effect, such as –CH_2–, led to an increase in the AET photosensitizer's efficiency-loaded ZnO and TiO_2NR photoanodes. Additionally, symbiotic structure with a considerably faster electron transport rate and effective light scattering phenomenon in TiO_2NR-based DSSC has been explained in detail. Enhanced to DSSC of TiO_2NR/AET is improved light absorption and decreased charge recombination at the photoanode/ photosensitizer /electrolyte interface. We believe our novel AET, 2-((thiophen-2-yl)ethylamino)-3-chloro-naphthalene-1,4-dione sensitized TiO_2NR based DSSC are simple and easy to scale up with the low cost.

Acknowledgments
Authors thankful to Department of Science and Technology, Government of India for financial support vide Sanction order DST/TMD/SERI/S173 (G).

Supporting Information
Applicable

Conflict of interest
There are no conflicts to declare.

References
[1] B. O'Regan and M. Grätzel, *Nature,* 1991, **353**, 737-740, doi: 10.1038/353737a0.
[2] X. Huang, P. Shen, B. Zhao, X. Feng, S. Jiang, H. Chen, H. Li, and S. Tan, *Sol. Energ. Mat. Sol. C.,* 2010, **94**, 1005-1010, doi: 10.1016/j.solmat.2010.02.005.
[3] R. N. Bulakhe, S. A. Arote, B. Kwon, S. Park and I. In, *Mater. Today Chem.*, 2020, **15**, 100210, doi: 10.1016/j.mtchem.2019.100210.
[4] R. N. Bulakhe, V. Q. Nguyen, D. Tuma, Y. R. Lee, H. Zhang, S. Zhang and J. J. Shim, *J. Ind. Eng. Chem.*, 2018, **66**, 288-297, doi: 10.1016/j.jiec.2018.05.043.
[5] D. Sinha, D. De, D. Goswami, A. Mondal and A. Ayaz, *Mater. Today*, 2019, **11**, 782-788, doi: 10.1016/j.matpr.2019.03.043.
[6] M. Grätzel, *J. Photochem. Photobiol. C: Photochem. Rev.*, 2003, **4**, 145-153, doi: 10.1016/S1389-5567(03)00026-1.
[7] M. Grätzel, *Accounts. Chem. Res.*, 2009, **42**, 1788-1798, doi: 10.1021/ar900141y.
[8] L. Giribabu and R. K. Kanaparthi, *Curr. Sci.*, 2013, **104**, 847-855.
[9] A. Mishra, M. K. R. Fischer and P. Bauerle, *Angew. Chem. Int. Edit.,* 2009, **48**, 2474 – 2499, doi: 10.1002/anie.200804709.
[10] H. Gerischer, M.E. Michel-Beyerle, F. Rebentrost and H. Tributsch, *Electrochim. Acta.*, 1968, **13**, 1509–1515, doi: 10.1016/0013-4686(68)80076-3.
[11] H. Gerischer, H. Tributsch and B. B. Ges, *Phys. Chem.*, 1968, **72**, 437–445, doi: 10.1002/bbpc.196800013.
[12] Y. Takekuma, T. Ochiai and M. Nagata, *Chem. Lett.,* 2018, **47**, 225–227, doi: 10.1246/cl.171024.
[13] H. Tsubomura, M. Matsumura, Y. Nomura and T. Amamiya, *Nature*, 1976, **261**, 402–403, doi: 10.1038/261402a0.
[14] S. Mathew, A. Yella, P. Gao, R. H. Baker, B. F. E. Curchod, N. A. Astani, I. Tavernelli, U. Rothlisberger, M. K. Nazeeruddin and M. Grätzel, *Nat. Chem.*, 2014, **6**, 242-247, doi: 10.1038/NCHEM.1861.
[15] Y. Hu, A. Abate, Y. Cao, A. Ivaturi, S. M. Zakeeruddin, M. Grätzel and N. Robertson, *J. Phys. Chem. C,* 2016, **120**, 15027-15034, doi: 10.1021/acs.jpcc.6b03610.
[16] I. P. Liu, W. N. Hung, H. Teng, S. Venkatesan, J. C. Lin and Y. L. Lee, *J. Mater. Chem. A,* 2017, **5**, 9190- 9197, doi: 10.1039/c7ta01341h.
[17] S. M. Gupta and M. Tripathi, *Chinese. Sci. Bul.,* 2011, **56**, 1639-1657, doi: 10.1007/s11434-011-4476-1.
[18] W. Kubo, S. Kambe, S. Nakade, T. Kitamura, K. Hanabusa, Y. Wada and S. Yanagida, *J. Phys. Chem. B,* 2003, **107**, 4374–4381, doi: 10.1021/jp034248x.
[19] B. S. Ito, S. M. Zakeeruddin, R. Humphry-Baker, P. Liska, R. Charvet, P. Comte, M. K. Nazeeruddin, P. Péchy, M. Takata, H. Miura, S. Uchida and M. Grätzel, *Adv. Mater.*, 2006, **18**, 1202–1205, doi: 10.1002/adma.200502540.
[20] Q. Huaulme, L. Cabau and R. Demadrille, *Chem,* 2018, **4**, 2260-2277, doi: 10.1016/j.chempr.2018.09.020.
[21] M. Zi, M. Zhu, L. Chen, H. Wei, X. Yang and B. Cao, *Ceram. Int.,* 2014, **40**, 7965-7970, doi: 10.1016/j.ceramint.2013.12.146.
[22] L. Wei, P. Wang, Y. Yang, Z. Zhan, Y. Dong, W. Song and R. Fan, *Inorg. Chem. Front.,* 2018, **5**, 54-62, doi: 10.1039/C7QI00503b.
[23] R. Zan, J. Xiao and X. Wen, *J. Mater. Sci: Mater. Electron.,* 2017, **28**, 4107-4113, doi: 10.1007/s10854-016-6030-z.
[24] A. E. Shalan, M. Rasly, I. Osama, M. M. Rashad and I. A. Ibrahim, *Ceram. Int.,* 2014, **40**, 11619-11626, doi: 10.1016/j.ceramint.2014.03.152.
[25] A. Hagfeldt, G. Boschloo , L. Sun , L. Kloo and H. Pettersson, *Chem. Rev.,* 2010, **110**, 6595-6663, doi: 10.1021/cr900356p.
[26] M. Zhang, Y. Wang, M. Xu, W. Ma, R. Li, and P. Wang, *Energy Environ. Sci.,* 2013, **6**, 2944, doi: 10.1039/C3EE42331J.
[27] K. Kakiage, Y. Aoyama, T. Yano, K. Oya, J. I. Fujisawa, and M. Hanaya, *Chem. Commun.*, 2015, **51**, 15894-15897, doi: 10.1039/C5CC06759f.
[28] A. Patil, A. P. Ware, S. Bhand, D. Chakravarty, R. Gonnade, S. S. Pingale and S. Salunke-Gawali, *J. Mol. Struct.,* 2016, **1114**, 132-143, doi: 10.1016/j.molstruc.2016.02.065.
[29] G. Agarwal, D. N. Lande, D. Chakrovarty, S. P. Gejji, P. Gosavi-Mirkute, A. Patil and S. Salunke-Gawali, *RSC. Adv.*, 2016, **6,** 88010-88029, doi: 10.1039/C6RA20970J.
[30] S. A. Mahadik, H. M. Pathan, S. Salunke-Gawali and R. J. Butcher, *J. Alloy. Compd.,* 2020, **845**, 156279, doi: 10.1016/j.jallcom.2020.156279.
[31] D. D. Perrin, W. Armarego and D. R. Perrin, *Pergamon Press, London,* 1988, p. 260.
[32] D. R. Burfield, and R. H. Smithers, *J. Org. Chem.,* 1983, **48**, 2420-2422, doi: 10.1021/jo00162a026.
[33] Bruker, APEX2, SAINT, SADABS: *Bruker AXS Inc., Madison, Wisconsin, USA.* 2007.
[34] G. M. Sheldrick, *Acta Crystallogr. A,* 2008, **A64**, 112- 122, doi: 10.1107/S0108767307043930.

[35] L. J. Farrugia, *J. Appl. Crystallogr.*, 2012, **45**, 849-854, doi: 10.1107/S0021889812029111.
[36] C. F. Macrae, I. J. Bruno, J.A. Chisholm, P. R. Edgington, P. McCabe, E. Pidcock, L. Rodriguez Monge, R. Taylor, J. van de Streek and P. A. Wood, *J. Appl. Crystallogr.*, 2008, **41**, 466-470, doi: 10.1107/S0021889807067908.
[37] A. L. Spek, *Acta Crystallogr.,* 2009, **D65**, 148-155, doi: 10.1107/S090744490804362x.
[38] S. S. Khadtare, A. P. Ware, S. Salunke-Gawali, S. R. Jadkar, S. S. Pingale and H. M. Pathan, *RSC Adv.,* 2015, **5**, 17647-17652, doi: 10.1039/C4RA14620d.
[39] S. S. Khadtare, S. R. Jadkar, S. Salunke – Gawali and H. M. Pathan, *J. Nanopart Res.,* 2013, **24**, 140-145, doi: 10.4028/www.scientific.net/JNanoR.24.140.
[40] Y. T. Yin and L. Y. Chen, *Energy Procedia,* 2014, **61**, 2042-2045, doi: 10.1016/j.egypro.2014.12.071.
[41] M. A. Mahadik, P. S. Shinde, M. Cho and J. S. Jang, *Appl. Catal.,* 2016, **184**, 337-346, doi: 10.1016/j.apcatb.2015.12.001.
[42] E. S. Aydil and B. J. Liu, *J. Am. Chem. Soc.,* 2009, **131**, 3985–3990, doi: 10.1021/ja8078972.
[43] P. K. Baviskar, J. B. Zhang, V. Gupta, S. Chand and B. R. Sankapal, *J. Alloy compd.,* 2012, **510**, 33-37, doi: 10.1016/j.jallcom.2011.08.034.
[44] O. Pawar, A. Patekar, A. Khan, L. Kathawate, S. Haram, G. Markad, V. Puranik and S. Salunke-Gawali, *J. Mol. Struct.,* 2014, **1059**, 68-74, doi: 10.1016/j.molstruc.2013.11.029.
[45] A. P. Ware, A. Patil, S. Khomane, T. Weyhermüller, S. S. Pingale and S. Salunke-Gawali, *J. Mol. Struct.,* 2015, **1093**, 39-48, doi: 10.1016/j.molstruc.2015.03.016.
[46] A. Patil, D. Lande, A. Nalkar, S. P. Gejji, D. Chakravarty, R. Gonnade, T. Moniz, M. Rangel, E. Periera and S. Salunke-Gawali, *J. Mol. Struct.,* 2017, **1143**, 495-514, doi: 10.1016/j.molstruc.2017.04.094.
[47] P. Gosavi-Mirkute, A. Patil, D. N. Lande, D. Chakravarty, S. P. Gejji, S. Satpute and S. Salunke-Gawali, *RSC Adv.,* 2017, **7**, 55163 – 55174, doi: 10.1039/c7ra10490a.
[48] G. W. An, M. A. Mahadik, W. S. Chae, H. G. Kim, M. Cho and J. S. Jang, *Appl. Surf. Sci.,* 2018, **440**, 688-699, doi: 10.1016/j.apsusc.2018.01.194.
[49] K. M. Samb-Joshi, Y. A. Sethi, A. A. Ambalkar, H. B. Sonawane, S. P. Rasale, R. P. Panmand, R. Patil, B. B. Kale and M. G. Chaskar, *J. Compos. Sci.,* 2019, **3**, 90, doi: 10.3390/jcs3030090.
[50] J. Wu, H. Lu, X. Zhang, F. Raziq, Y. Qu and L. Jing, *Chem. Commun.,* 2016, **52**, 5027-5029, doi: 10.1039/c6cc00772d.
[51] S. S. Kumbhar, M. A. Mahadik, V. S. Mohite, Y. M. Hunge, K. Y. Rajpure and C. H. Bhosale, *Mater. Res. Bull.,* 2015, **67**, 47–54, doi: 10.1016/j.materresbull.2015.02.056.
[52] G. W. An, M. A. Mahadik, W. S Chae, H. G. Kim, M. Cho and J. S. Jang, *Appl. Surf. Sci*., 2018, **440**, 688-699, doi: 10.1016/j.apsusc.2018.01.194.
[53] N. I. Beedri, P. K. Baviskar, M. A. Mahadik, S. R. Jadkar, J. S. Jang and H. M. Pathan, *Eng. Sci.,* 2019, **8**, 76-82, doi: 10.30919/es8d803.
[54] S. Majumder, P. K. Baviskar and B. R. Sankapal, *Electrochim. Acta,* 2016, **222**, 100-107, doi: 10.1016/j.electacta.2016.10.147.
[55] K. D. Seo, B. S. You, I. T. Choi, M. J. Ju, M. You, H. S. Kang and H. K. Kim, *J. Mater. Chem. A,* 2013, **1**, 9947–9953, doi: 10.1039/c3ta11832k.
[56] K. S. Pawar, P. K. Baviskar, Inamuddin, Altafhusain B, S. Salunke-Gawali and H. M. Pathan, *Mater. Renew. Sustain. Energy,* 2019, **8**, 12, doi: 10.1007/s40243-019-0148-x.
[57] M. Urbani, M. Grätzel, M. K. Nazeeruddin and T. Torres, *Chem. Rev.*, 2014, **114**, 12330-12396, doi: 10.1021/cr5001964.
[58] S. Qu, C. Qin, A. Islam, Y. Wu, W. Zhu, J. Hua, H. Tian and L. Han, *Chem. Commun*., 2012, **48**, 6972-6974, doi: 10.1039/c2cc31998e.
[59] S. M. Feldt, E. A. Gibson, E. Gabrielsson, L. Sun, G. Boschloo and A. Hagfeldt, *J. Am. Chem. Soc.*, 2010, **132**, 16714-16724, doi: 10.1021/ja1088869.
[60] M. Liang and J. Chen, *Chem. Soc. Rev*., 2013, **42**, 3453-3488, doi: 10.1039/c3cs35372a.
[61] L. L. Li and E. W. G. Diau, *Chem. Soc. Rev*., 2013, **42**, 291-304, doi: 10.1039/c2cs35257e.
[62] K. Khanmohammadi, B. Sohrabi and M.R. Zamani Meymian, *J. Mol. Struct.,* 2018, **1167**, 274-279, doi: 10.1016/j.molstruc.2018.05.014.
[63] M. J. Jeng, Y. L. Wung, L. B. Chang, and L. Chow, *Int. J. photoenergy,* 2013, 6346, doi: 10.1155/2013/563897.
[64] J. Yoon, M. Jin and M. Lee, *Adv. Mater.,* 2011, **23**, 3974-3978, doi: 10.1002/adma.201101837.
[65] Y. Li, Q. Tang, L. Yu, X. Yan and L. Dong, *J. Power Sources,* 2016, **305**, 217-224, doi: 10.1016/j.jpowsour.2015.11.063.
[66] M. Eslamian, *Coatings*, 2014, **4**, 60-84, doi: 10.3390/coatings4010060.
[67] S. Peng, G. Jin, L. Li, K. Li, M. Srinivasan and S. Ramakrishna, *J. Chen, Chem. Soc. Rev.,* 2016, **45**, 1225-1241, doi: 10.1039/c5cs00777a.
[68] D. Wongratanaphisan, K. Kaewyai, S. Choopun, A. Gardchareon, P. Ruankham and S. Phadungdhitidhada, *Appl. Surf. Sci.,* 2019, **474**, 85–90, doi: 10.1016/j.apsusc.2018.05.037.
[69] M. N. Mustafa, S. Shafie, M. H. Wahid and Y. Sulaiman, *Sci. Rep.*, 2019, **9**, 14952, doi: 10.1038/s41598-019-50292-z.
[70] R. Gao, Z. Liang, J. Tian, Q. Zhang, L. Wang and Guozhong, *RSC Adv.,* 2013, **3**, 18537-18543, doi: 10.1039/c3ra41827h.

[71] Q. Zhang, C. S. Dandeneau, X. Zhou and G. Cao, *Adv Mater,* 2009, **21**, 4087-4108, doi: org/10.1002/adma.200803827.
[72] M. Yoon, J. A. Chang, Y. Kim, J. R. Choi, K. Kim and S. J. Lee, *J. Phys. Chem. B,* 2001, **105**, 2539-2545, doi: 10.1021/jp003736r.
[73] L. Wang, M. A. Mamun, P. Liu, Y. Wang, H. G. Yang, H. F. Wang and H. Zhao, *NPG Asia Mater.,* 2015, **7**, 226, doi: org/10.1038/am.2015.121.

Author information

Sharad A. Mahadik *is Ph.D. student under guidance of Professor Sunita Salunke – Gawali and Dr. Habib M. Pathan at Department of Chemistry Savitribai Phule Pune University, Pune (India). He received his master's in Organic Chemistry in 2013, and B.Ed. (Bachelor of Education) in 2016. His research interests are, synthesis of photosensitizers and photoanodes in dye sensitized solar cells.*

Amit Patil *is Ph.D. student under guidance of Professor Sunita Salunke - Gawali at Savitribai Phule Pune University, Pune (India). He received his master's in Organic Chemistry in 2012, and M.Phil. in 2016. His research interests are, synthesis of chemosensor ligands and transition metal complexes of naphthoquinone derivatives.*

Sunita Salunke-Gawali *is Professor at Department of Chemistry, Savitribai Phule Pune University since 2008. She did her Ph.D. (1999) at Pune University, she worked as Post-doctoral Research Associate at Laboratoire de Magnétisme et d'Optique, Versailles France (Prof. F. Varret, 2001-2002), Department of Chemistry, IIT Bombay, India (Prof. C.P. Rao, 2002 and 2004), Universidade do Porto, Portugal, supervised by Prof. Eulália Pereira (2004-2007) and Max-Planck-Institut für Bioanorganische Chemie, Mülheim an der Ruhr, Germany (Dr. Eckhard Bill, 2007- 2008). Her research interests are coordination and bioorganic Chemistry of naphthoquinone ligands, developing photosensitizer for DSSC, HPLC method development for anticancer drugs and organic tautomers, chemosensors and metallosurfactants. She is the author of more than 86 articles in international journals.*

Habib M. Pathan *received his Ph.D. in 2003 from Shivaji University, Kolhapur, India. Afterwards, he joined with Prof. Oh-Shim Joo at the Korea Institute of Science and Technology Seoul, South Korea, as a post-doctoral fellow in 2004. He is Associate professor in Physics at the department of Physics Savitribai Phule Pune University Pune, India His research is focused on material science, energy conversion and storage. He is the author of more than 150 articles in international journals. He is founding Executive Editorial board of ES Energy & Environment and ES Materials and Manufacturing.*

Ray J. Butcher *born in Greymouth, New Zealand on 11th October 1945. Educated at the University of Canterbury in New Zealand. Appointed Instructor 1974-76 at the University of Virginia, Charlottesville, Virginia and Post-Doctoral Fellow 1976-77, Georgetown University, Washington D.C. Joined the Chemistry Department at Howard University as an Assistant Professor in 1977 and promoted to Associate Professor in 1982 and Professor in 1997. Has had many visiting appointments including as a Navy Distinguished Summer Faculty Fellow at the Naval Research Laboratory, a Visiting Senior Scientist at Los Alamos National Laboratory, Los Alamos, a Distinguished Visiting Professor at the Indian Institute of Technology Bombay, in Mumbai, India. Has held two Fulbright-Nehru Fellowships to India (1989, 2009) and a Distinguished Chair Fulbright-Nehru Fellowship to India (2019). Was elected a Fellow of the Royal Society of Chemists (FRSC) in 2018. Has published over 1340 papers in refereed journals since 1975.*

